Design of a high gain single stage and single pass Nd:YVO4 passive picosecond amplifier

Xavier Délen, François Balembois, Patrick Georges

Design of a high gain single stage and single pass Nd:YVO$_4$ passive picosecond amplifier

Xavier Délen,* François Balembois, and Patrick Georges

Laboratoire Charles Fabry, Institut d'Optique, CNRS, Univ Paris-Sud, 2 Av A. Fresnel, 91127 Palaiseau CEDEX, France
*Corresponding author: xavier.delen@institutoptique.fr

A detailed comparison of the influence of pumping wavelength and crystal doping concentration on the performance of Nd:YVO$_4$ amplifiers is developed through theoretical analysis. The effect of energy transfer upconversion and the strong temperature dependence of the emission cross section were taken into account. This study showed the interest of 808 nm pumping with low doping concentration crystals and the importance of the crystal temperature for the design of a high gain amplifier. Using these conclusions, we built a picosecond Nd:YVO$_4$ master oscillator power amplifier reaching 10 W output power for only 50 mW of seed at 200 kHz in a single pass, single stage configuration. With a pulse duration of 22 ps, it corresponds to an output pulse energy of 50 μJ and to a peak power of 2.3 MW. With a same setup, a single pass small signal gain over 45 dB has been measured, and near 50% extraction efficiency was reached for a seed power of 3.5 W. The influence of the Nd:YVO$_4$ amplifier temperature on the output power was also studied for different levels of gain saturation. © 2012 Optical Society of America

OCIS codes: 140.3280, 140.3430, 140.3530, 140.3613.

1. INTRODUCTION

Picosecond laser emitting pulses in the tens of microjoules regime and working at hundreds of kilohertz repetition rates are in high demand in fields such as material processing. There are many different laser architectures that can be used to obtain such a source. Although a high power has been reached in the picosecond regime, systems based on fiber technology are limited in terms of peak power [1]. Ultralow repetition rate oscillators, as low as 1 MHz, can be developed [2], but those very long cavities are difficult to handle, leading to poor long-term stability. An alternative solution to access these regimes is mode locked cavity dumping, which has proven to be a successful technique. However, the output power decreased quickly with the repetition rate below 1 MHz [3]. A master oscillator power amplifier (MOPA) combining a picosecond oscillator and a regenerative amplifier is often used in order to work at a lower repetition rate [4–6]. Regenerative amplifiers allow large repetition rate flexibility and good extraction efficiency without requiring a high energy level for the seed signal. The disadvantage of this solution is the complexity and the cost of the system. A passive amplifier, with a single pass in a single stage, can be considered as a simple and elegant solution if the gain of the medium is high enough. It can be the case for Nd doped yttrium vanadate crystal (Nd:YVO$_4$) thanks to its huge cross section of $12\ 10^{-19}$ cm^2 at 1064 nm. As an example, very high gain of around 50 dB has already been demonstrated in two stages Nd:YVO$_4$ grazing incidence slabs amplifier, showing the potential of direct amplification of a pulsed picked picosecond laser [7]. However, this system was working under quasi-continuous wave (qcw) pumping at low repetition rate (100 Hz) with a low extraction efficiency below 1%. High repetition rate operation requires the use of cw pumping and increases considerably the thermal load in the crystal. This induces deleterious effects on the amplification performance: recent work showed that the

emission cross section of the π polarized 1064 nm line in Nd doped vanadate crystals decays rapidly with temperature [8–10]. This comes from both the emission line broadening and the spectral shift, which induces a detuning between the oscillator and the amplifier. The spectral shift is around 3 pm/°C, whereas the emission linewidth at 1064 nm at room temperature is around 0.7 nm FWHM. As much as a 50% decrease of the emission cross section has been observed at a fixed wavelength for a temperature increase of only 60 K. Consequently, the design of a simple and efficient Nd:YVO$_4$ amplifier operating at high repetition rate and high pump power level is challenging. To design such an amplifier, we propose some theoretical guidelines including a study of the influence of doping concentration and a theoretical comparison between several possible pumping wavelengths for high gain systems. We take into account the influence of concentration quenching and energy transfer upconversion (ETU) and the strong temperature dependence of the emission cross section. In the second part, we propose an experimental illustration with a longitudinally pumped single pass and single stage amplifier seeded by a pulse picked picosecond mode locked oscillator.

2. THEORETICAL GUIDELINES

The following sections describe theoretical calculations that are used to illustrate general trends in Nd:YVO$_4$ amplifiers using data and models available in the literature. Although several papers have been published on fluorescence quenching and ETU, there is a relatively wide uncertainty on the values measured in Nd:YVO$_4$, and our calculations are meant to study trends and not to calculate precise quantitative data.

A. Influence of the Doping Concentration
In order to reach a high gain and a high extraction efficiency in the amplifier, both a high inversion of population and a high

emission cross section are required. Several processes can lead to nonradiative decays and therefore to a reduction of the upper level population. First of all, migration of excitation coupled with radiation trapping as well as cross relaxation are responsible for the concentration quenching effect. The probability of these decays increases with the doping concentration. This results in shorter excited state lifetime for highly doped samples and can be modeled in rate equations with a term similar to the one of spontaneous emission. Another process limiting the upper level population is ETU, which is due to an energy transfer between two ions in the excited state and results in the loss of one excited state ion energy. This transition probability increases with inversion of population and the doping concentration. In the case of migration assisted ETU, it can be modeled adding a quadratic term γn^2 in the rate equation (1) giving the rate equation for the upper level in the case of an ideal four level system [11].

$$\frac{dn}{dt} = -\frac{n}{\tau_{\text{sp}}} - \frac{n}{\tau_{\text{nr}}} - \gamma n^2 + R - \sigma I, \qquad (1)$$

where n is the upper level population, τ_{sp} is the radiative lifetime, τ_{nr} is the nonradiative lifetime, γ is the upconversion coefficient, R is the pumping rate, σ is the laser emission cross section, and I is the laser intensity. According to the literature, the inverse of the nonradiative lifetime increases quadratically with the doping concentration following Eq. (2) [12].

$$\frac{1}{\tau_{\text{nr}}} = \frac{1}{\tau_{\text{sp}}}\left(\frac{C}{C_q}\right)^2, \qquad (2)$$

where C_q is the concentration quenching parameter and C is the doping concentration in atomic percentage. For Nd:YVO$_4$, a value of $C_q = 3.1$ is given in the literature for a τ_{sp} of 107 μs [12]. Three different values can be found for the upconversion coefficient in Nd:YVO$_4$ at three different doping concentrations: $1.5\,10^{-21}$ m^3/s for 0.5% doping concentration [11], $3\,10^{-21}$ m^3/s for 1% doping concentration [13], and $7\,10^{-21}$ m^3/s for 1.5% doping concentration [14]. Assuming that a linear evolution of the ETU coefficient with the doping concentration is also verified for Nd doped vanadate, as has been observed for other Nd doped crystals [15,16], an average upconversion coefficient per atomic percentage of doping concentration of $3.6\,10^{-21}$ m^3/s/at.% can be deduced.

In order to compare the performance that can be obtained with different Nd^{3+} doping concentrations, we can define the effective lifetime of the laser transition upper level for a defined inversion of population τ_{eff} as given in Eq. (3). This effective lifetime seems to be a good parameter for a comparison between different doping concentrations in high gain amplifiers. Figure 1 shows the effective lifetime as a function of the doping concentration in atomic percentage for different population inversions. In order to describe general concepts, we define the upper electronic level population in atomic percentage $n^\%$ similarly as a doping concentration : $n^\%$ is defined as the ratio between the excited ions density n and the ions density for a 1% atomic concentration $n_t^{1\%}$ as described by Eq. (4). For example, a population of $n^\% = 0.05\%$ corresponds to an excited population being half the total population in a 0.1% doped crystal and to 10% of the total population in a 0.5% doped crystal. When there is no inversion of population,
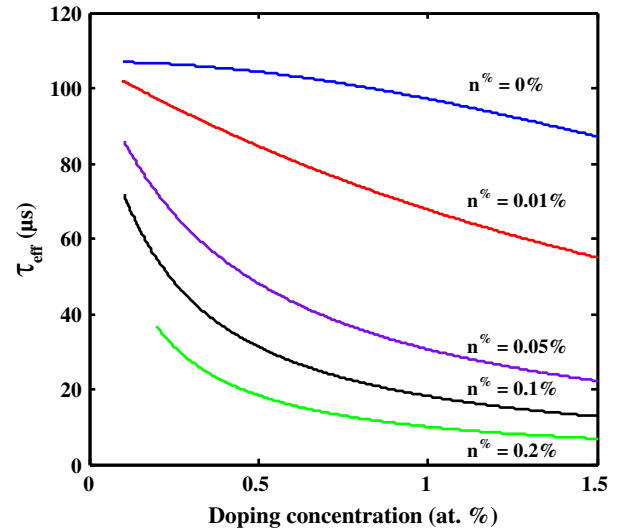

Fig. 1. (Color online) Effective excited state lifetime as a function of the doping concentration for different upper level population densities.

the effective lifetime decrease is only due to concentration quenching, but it decreases quickly with the inversion of population because of ETU. For a 0.1% doping concentration, the effective lifetime varies between 107 μs and 72 μs for a population inversion between 0% and 0.1%, whereas it is between 104 and 31 μs for a 0.5% doping concentration and the same range of inversion of population. Considering high inversion of population of 0.2 at. %, the maximal effective lifetime is only 37 μs. All these elements show that using a Nd:YVO$_4$ crystal at a high level of inversion of population is in general very difficult to achieve, but it is easier using a low doping concentration. A major advantage of low doping concentration is that the inversion of population is intrinsically limited to a low value by the total population. Indeed, the saturation of absorption will induce a decrease of the absorption as the inversion of population increases.

$$\frac{1}{\tau_{\text{eff}}} = \frac{1}{\tau_{\text{sp}}} + \frac{1}{\tau_{\text{nr}}} + \gamma n, \qquad (3)$$

$$n^\% = \frac{n}{n_t^{1\%}}. \qquad (4)$$

B. Influence of the Pumping Wavelength

Working with Nd:YVO$_4$ at high pump power, 880, 888, and 914 nm pumping wavelengths have been used in order to reduce the quantum defect and therefore the associated heat load [17–19]. The drawback with these pumping wavelengths is the low absorption, which is usually compensated by the use of higher doping concentration and longer crystals. Extra heat generation is associated to nonradiative decays and the different pumping wavelengths should be compared in terms of total heat load density and not only quantum effect. Indeed, as the doping concentration has to be increased for 880, 888, or 914 nm pumping wavelengths, the extra heat load associated to nonradiative decays will be larger for a given population inversion. As the effective upper state lifetime also decreases strongly with the doping concentration, a higher

pumping rate will also have to be used to reach a given level of inversion of population. The heat load density Q in watts per unit of volume can be calculated using Eq. (5), where σ is the emission cross section at the laser wavelength, I is the laser intensity, λ_p is the pumping wavelength (808, 880, or 888 nm), λ_l is the laser wavelength (1064 nm), and λ_f is the average fluorescence wavelength (1032 nm) [12].

$$Q = \frac{hc}{\lambda_p}\left(\frac{n}{\tau_{nr}} + \gamma n^2\right) + \left(\frac{hc}{\lambda_p} - \frac{hc}{\lambda_f}\right)\frac{n}{\tau_{sp}} + \left(\frac{hc}{\lambda_p} - \frac{hc}{\lambda_l}\right)\sigma In. \quad (5)$$

We considered doping concentrations of 0.1%, 0.3%, and 0.5% for 808, 880, and 888 nm pumping wavelengths, respectively. They correspond to typical doping concentrations that are referred to in the literature. For each population inversion, we calculated the heat load for a reference ideal case with 808 nm pumping without nonradiative transitions as given by Eq. (6) and used Eq. (7) to calculate the normalized heat load density Q_{norm} as a function of the inversion of population (Fig. 2). This was done for the three different pumping wavelengths and their corresponding doping concentrations but also for different levels of laser intensity. In order to define
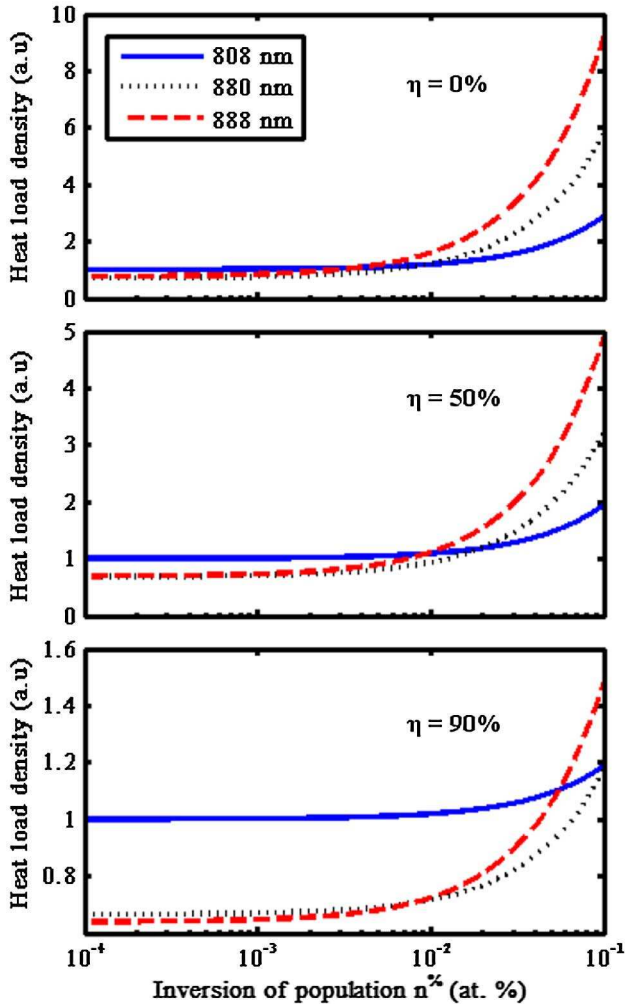

Fig. 2. (Color online) Normalized heat load density Q_{norm} as a function of the population inversion for different extraction efficiencies.

general concepts, we consider decay rates by stimulated emission corresponding to quantum extraction efficiencies η of 0%, 50%, and 90% defined for an ideal crystal without concentration quenching nor ETU [Eq. (8)]. Without any laser extraction, the heat load density is minimal for 808 nm pumping for an inversion above 0.01 at. %. Even for the case of a 50% extraction, 808 nm pumping appears as the pumping wavelength for which the heat load density is the lowest for inversion of population above 0.02 at. %. However, the advantage of higher pumping wavelength such as 880 or 888 nm is clear for low inversion of population and high extraction rates as shown by the results obtained for $\eta = 90\%$. In this last case, most decays are due to stimulated emission transitions at the laser wavelength, and the major part of the heat load is due to the quantum defect.

$$Q_{ref} = \left(\frac{hc}{\lambda_p} - \frac{hc}{\lambda_f}\right)\frac{n}{\tau_{sp}} + \left(\frac{hc}{\lambda_p} - \frac{hc}{\lambda_l}\right)\sigma In \quad \text{with } \lambda_p = 808 \text{ nm},$$
$$(6)$$

$$Q_{norm} = \frac{Q}{Q_{ref}}, \quad (7)$$

$$\eta = \frac{\sigma In}{\frac{n}{\tau_{sp}} + \sigma In}. \quad (8)$$

C. Influence of the Temperature

The extra heat load associated to nonradiative transitions does not only induce stronger thermal lenses but also changes the spectroscopic properties of the laser material. Especially, the emission cross section at 1064 nm strongly decreases with temperature [8–10]. As a consequence, nonradiative transitions will induce a gain reduction not only due to the population depletion but also due to the temperature increase. In order to obtain the small signal gain coefficient given by Eq. (9), we first need to calculate the population inversion using Eq. (10), where R is the pumping rate defined as the number of absorbed pump photons per unit of time and volume. The heat load density can then be deduced with Eq. (5) and used to evaluate the temperature increase in the crystal. Assuming a radial heat transfer, a top hat pump beam of $r_p = 200$ μm radius, and a crystal diameter of 3 mm ($r_c = 1.5$ mm), the temperature difference between the center and the edge of the crystal can be calculated analytically [Eq. (11)] [20]. To simplify our model and be able to use this analytic expression of the temperature, we used an average value of the thermal conductivity K_c of 10 W/m/K not accounting for the anisotropy of YVO$_4$ [21,22]. At first, we only considered the temperature increase inside the crystal ΔT_c and assumed a perfect contact between heat sink and crystal. The emission cross section at a fixed wavelength of 1064.1 nm for pi polarization was deduced from the formula given by Sato and Taira [10]. Figure 3 shows the evolution of the small signal gain coefficient as a function of the pumping rate for different pumping wavelengths assuming a doping concentration of, respectively, 0.1%, 0.3%, and 0.5% for 808, 880, and 888 nm pumping. In order to emphasize tendencies, g0 was normalized to its maximum value and R to a reference value $R_{ref} = 1.4 \, 10^{29}$ s^{-1}m^{-3} corresponding to 50 W on 400 μm diameter and a 0.1% doped crystal in stationary state. It shows a
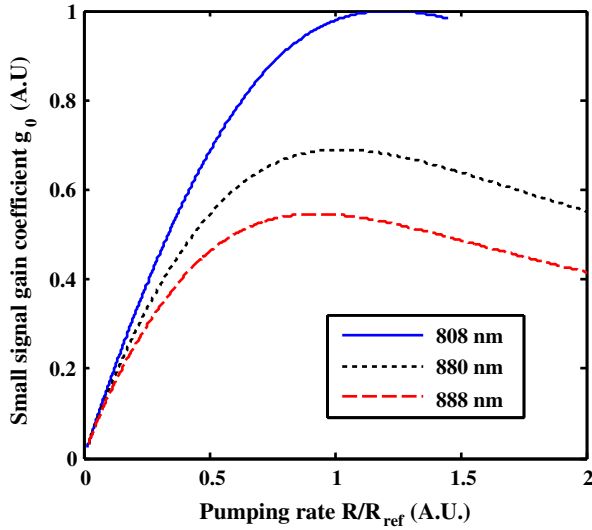
Fig. 3.   (Color online) Small signal gain coefficient as a function of the pumping rate for 808 nm (0.1%), 880 nm (0.3%), and 888 nm (0.5%) pumping.

Fig. 4.   (Color online) Small signal gain coefficient as a function of k for different pumping rates.

linear increase of the gain with pumping rate for low pumping rate levels at which nonradiative decays are negligible. At higher rates, the slope starts decreasing due to the emission cross section decrease with the temperature increase associated to higher pumping rates. For 880 and 888 nm pumping, the decrease is more significant due to both the emission cross section decrease and the population depletion induced by ETU. Our model even shows a decrease of the small signal gain coefficient for high pumping rates. The maximum small signal gains reached for 880 and 888 nm pumping are, respectively, 30% and 45% lower than the maximum reached for 808 nm pumping. Although it appears counterintuitive at first because of the higher quantum defect, these calculations show a clear advantage for 808 nm pumping under high inversion of population. The high absorption at this pumping wavelength allows the use of low doping concentration at which nonradiative decays are less probable thanks to the higher interion distances. It is then easier to reach high small signal gain using 808 nm pumping because of higher effective excited state lifetime.

$$g_0 = \sigma(T)n_0(R), \tag{9}$$

$$n_0 = \frac{1}{2\gamma}\left[-\frac{1}{\tau_{sp}} - \frac{1}{\tau_{nr}} + \sqrt{\left(\frac{1}{\tau_{sp}} + \frac{1}{\tau_{nr}}\right)^2 + 4\gamma R}\right], \tag{10}$$

$$\Delta T_c = \frac{Q r_p^2}{4 K_c}\left[\ln\left(\frac{r_c^2}{r_b^2}\right) + 1\right]. \tag{11}$$

In order to maintain a low temperature inside the crystal to benefit from a high emission cross section, it is not only essential to limit the heat load associated to nonradiative effects, but it is also very important to obtain a good thermal contact between the crystal and the heat sink and to optimize the cooling system. Indeed, the gain in Nd:YVO$_4$ depends on the absolute temperature and not on the temperature gradient
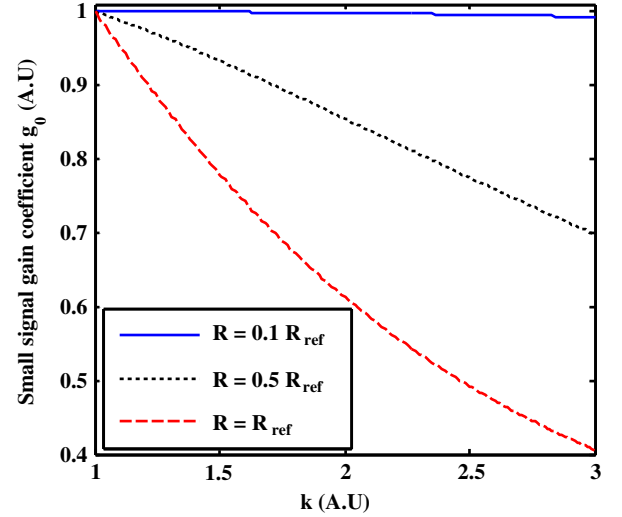
inside the crystal like thermal lensing effects. Considering a water cooled system for example; we can distinguish the total temperature difference between the center of the pumped crystal T_c and the incoming water T_w and the intrinsic temperature increase inside the crystal between the center and the crystal edge T_e. In order to illustrate the importance of these parameters, we can define a simple parameter modeling the cooling system quality k given by Eq. (12). For a water cooled system, we can anticipate typical k values ranging between 1.1 and 1.5 depending on the contact quality between crystal and heat sink [23]. Considering air-cooled systems, much larger k values can be anticipated, depending on the system. Figure 4 shows the relative variations of the small signal gain coefficient as a function of this parameter for three different pumping rates. For a fixed water temperature of 5 °C, given k and R we calculated the temperature in the center of the crystal using Eqs. (11) and (12), the temperature dependent cross section and the small signal gain. At low pumping rates, the heat load stays small and the cooling system quality has a very weak influence on the small signal gain. However, considering high pumping rates, the cooling system quality has a huge impact on the small signal gain coefficient showing the large influence of technological choices for the cooling system of an amplifier.

$$k = \frac{T_c - T_w}{T_c - T_e}. \tag{12}$$

To summarize, our theoretical approach shows clearly that 808 nm pumping is more efficient as far as significant gain is requested. Moreover, the study shows the deleterious effect of temperature increase on the gain, meaning that crystal cooling needs to be considered carefully.

3. EXPERIMENT

A. Setup

In order to illustrate the high potential of low doping concentration Nd:YVO$_4$ pumped at 808 nm and its use as a high gain amplifier, we have built a simple amplifier setup. Figure 5 shows the experimental setup used for this work. The amplifier
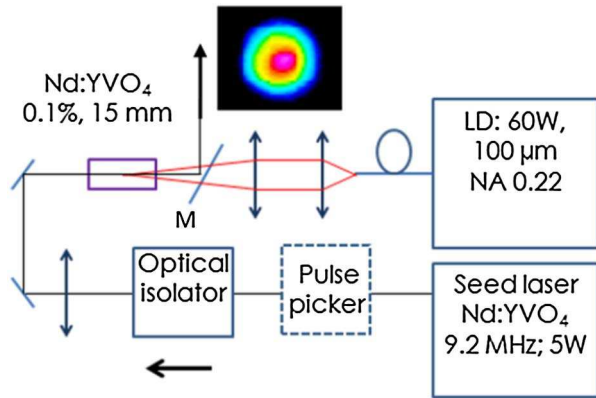
Fig. 5. (Color online) Experimental setup of our single stage, single pass amplifier. LD stands for laser diode. Beam profile obtained for a maximum pump power and a seed of 50 mW at 200 kHz repetition rate.

was kept as simple as possible with a single pass for both the pump and the signal in longitudinal contrapropagative pumping configuration. As shown in Section 2, a low doping concentration allows us to reduce nonradiative effects and to spread the heat load over a longer length and to reduce the absolute temperature increase in the crystal. This way, the emission cross section decrease and the gain spectral shift of the amplifier are limited. The two crystal faces were coated with an anti-reflective coating highly transparent at 808 nm and at 1064 nm ($R < 0.1\%$). A high brightness fiber coupled laser diode emitting a maximum output power of 60 W at 808 nm out of a 100 μm 0.22 NA fiber corresponding to a pump beam M^2 of 43 was used for pumping. Using two doublets of focal length 60 and 200 mm, the pump light was collimated and focused into the laser crystal over an expected diameter of 330 μm given by the fiber core diameter and the magnification. The exact position of the pump waist along the optical axis was chosen in order to maximize the performance. The pump absorption was 75%. The active medium was a 15 mm long and 0.1% doped Nd:YVO$_4$ crystal mounted between two water cooled heat sinks using indium foils carefully design to limit the temperature difference between the crystal and its mount. In order to test the efficiency of our cooling system, we used a setup very similar to the one used by Chénais *et al.* [23]; a thermal camera and a ZnSe dichroïc beam splitter were used to obtain the temperature map of the crystal in order to monitor the thermal contact quality while mounting the crystal. For about 50 W of incident pump power on a spot diameter around 330 μm, the crystal edges were measured to be about 30 °C above water temperature. The temperature gradient between the edge and the center of the crystal was around 40 °C. A heat transfer coefficient of 0.7 W/cm^2/K can be estimated using these two values. This is close to the value of 0.9 W/cm^2/K measured with indium foil contact during a previous study [23].

In order to start the amplification process with significant pulse energy, we designed a long cavity picosecond oscillator [2,3]. It included a Herriot-style multiple-pass cavity (MPC) made of two large mirrors (plane mirror and $R = 4$ m), leading to a 16.3 m long cavity and to a repetition rate of 9.2 MHz. Passive modelocking was obtained using a semiconductor saturable absorber (SESAM) with a saturation fluence of 70 μJ/cm^2 and a modulation depth of 1.2%. The gain medium was a $3 \times 3 \times 10$ mm Nd:YVO$_4$ crystal with a doping concentration of 0.1% pumped at 30 W by a fiber coupled laser diode

at 808 nm (400 μm core diameter 0.22 NA). For an output coupler transmission of 15%, the oscillator delivered more than 5 W of output power with a pulse energy of 0.54 μJ and a pulse duration of 22 ps. The output beam was nearly diffraction limited with an M^2 value below 1.3 measured using the second moment width.

Before amplification, we used an acousto-optic modulator as a pulse peaker in order to decrease the repetition rate. The signal beam was sent in the amplifier in contrapropagative configuration with respect to the pump, and its waist diameter was 400 μm in the crystal. The input polarization of the signal beam was adjusted using a half wave-plate. The flat dichroïc mirror M at the output of the amplifier was HR coated for 1064 nm and HT coated for 808 nm for an incidence angle of 45°. The absorbed pump power was monitored during the experiment. Due to the extremely high gain that can be obtained in the crystal at high pump power, we observed parasitic oscillation between the two faces of the Nd:YVO$_4$ without seed power, despite their antireflection coating. For a maximum pump power and a pump beam perpendicular to the two crystal faces, the parasitic laser effect was observed at 1064 nm. In order to separate this laser effect from the amplified signal and be able to make sure the parasitic oscillation disappears with the signal seeding, the laser crystal was slightly tilted by about 2° so that the amplified beam and the parasitic laser beam were angularly separated.

B. Experimental Results
At first, the pulses were seeded at full repetition rate (9.2 MHz) without the pulse picker in order to be able to study the performance of the amplifier for a wide range of input powers. The evolution of the output power as a function of the injected power was measured for injected power ranging between 26 mW and 3.5 W, as shown in Fig. 6. The parasitic laser effect was observed for injected power below 26 mW. Because of the gain saturation, this parasitic laser effect disappeared at higher signal level. During this experiment, the temperature of the water in the cooling system of the crystal was set at 5 °C. With an output power of 8.9 W, a maximum gain of about
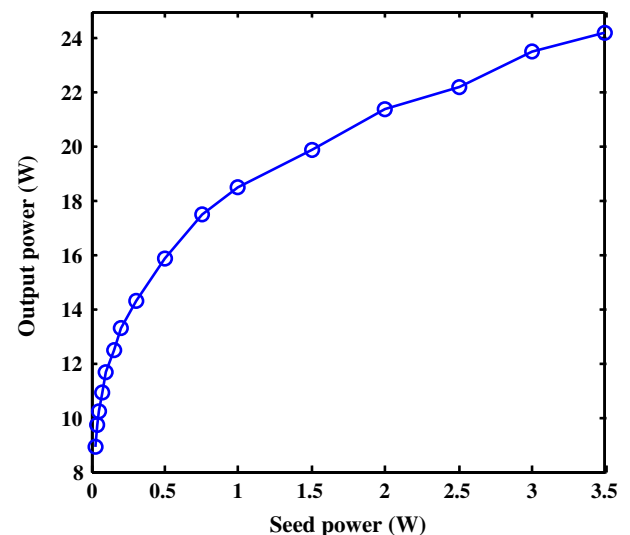

Fig. 6. (Color online) Output power as a function of the seed power for a repetition rate of 9.2 MHz and a cooling water temperature of 5 °C.
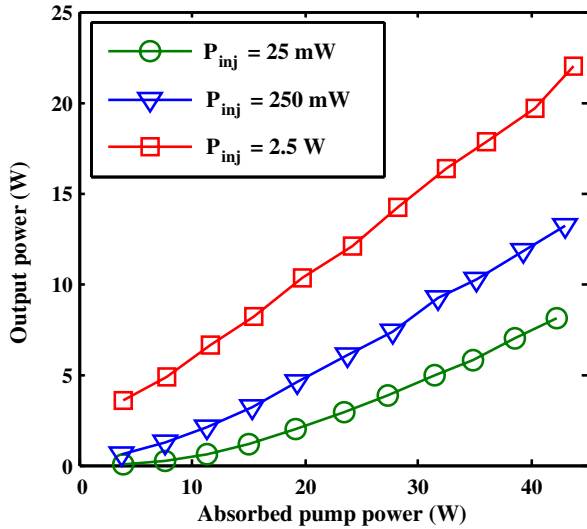
Fig. 7.   (Color online) Output power as a function of the absorbed pump power for a repetition rate of 9.2 MHz and a cooling water temperature of 17 °C.

440 corresponding to 26 dB was measured for an injected power of 26 mW. In this configuration, the total absorbed power was 40.5 W, resulting in an extraction efficiency of 22%. It reached 49% for 3.5 W injected power and 24.2 W of output power. Due to the increase of the extraction efficiency with the injected power, the inversion of population decreased and the saturation of absorption was reduced for the pump. This resulted in an increase of 5% of the absorbed pump power for a seed power increasing from 26 mW to 3.5 W. In Fig. 7, we show the output power as a function of the absorbed pump power for three different values of the seeded power. This time, the cooling temperature was set at 17 °C in order to avoid water condensation on the crystal faces at low pump power. The three curves do not show any sign of rollover, which indicates a limited effect of the temperature increase. Deleterious effects of temperature increase induced by the pump are kept under control in our setup. The foregoing also reveals the potential of this type of system at higher pump power level.
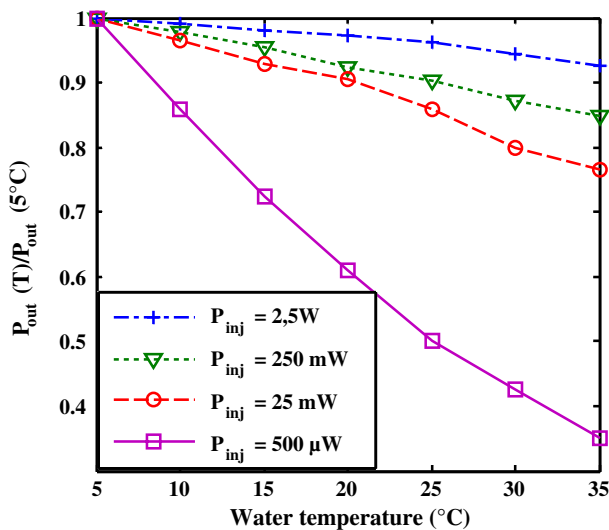
Figure 8 shows the evolution of the output power with the temperature of the water circulating in the heat sinks. Variations of the absorbed pump power were also observed with the temperature. They can be induced by the lower extraction level, which results in a saturation decrease, but also by absorption cross section variation at the pump wavelength. In order to compensate for these effects, the pump power was adjusted to operate at a fixed absorbed pump power of 38 W. The results are shown for four levels of injected pump power: 25 mW, 250 mW, and 2.5 W. For a high saturation of the gain, the output power decrease was only of about 7% for a temperature increase of 30 °C. However, this decrease reached respectively 15%, 24%, and 65% for input power of 250 mW, 25 mW, and 500 μW. The influence of the temperature on the output power varies strongly with the gain saturation level. It is most important for the low saturation regime close to the small signal gain regime. This result shows the significant impact of temperature on such a high gain system and the influence of the gain saturation level on this decrease similar to observations done in Nd:YVO$_4$ oscillators [9].

In order to be able to study the evolution of the gain with a weak seed power, we increased the tilt of the crystal to 15°. This way, it was possible to work at maximum pump power without observing any parasitic laser effect. It also minimized the power extraction of the beam reflected by the antireflective coating of the crystal. The seed power was modulated using a half wave-plate and a polarizer. Several diaphragms were used in order to minimize the collection of amplified spontaneous emission and fluorescence by our power meter. Figure 9 shows the gain in decibels as a function of the seed power, which is given in watts. The small signal gain is larger than 45 dB. Considering a Gaussian beam profile for both the pump and the signal and adjusting the beam divergence according to the beam M^2, we performed numerical resolution of rate equations in order to calculate the expected small signal gain in our system using the method described in [14]. We did this calculation for an ideal case without taking into account ETU or the temperature dependance of the emission cross section and found an expected small signal gain

Fig. 8.   (Color online) Evolution of the output power with the cooling temperature of the amplifier crystal for a repetition rate of 9.2 MHz.
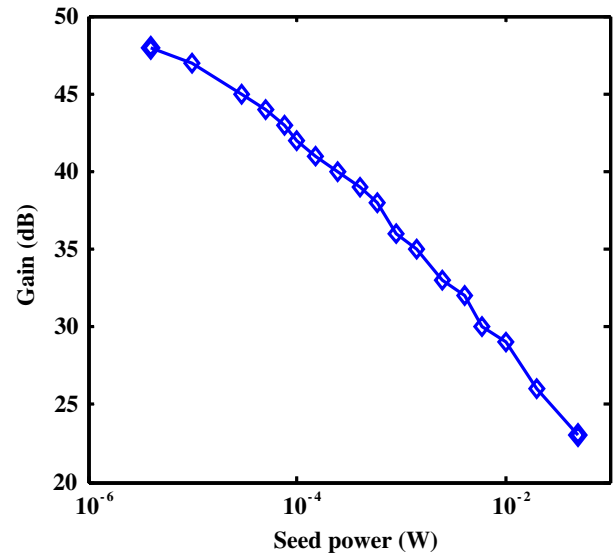

Fig. 9.   (Color online) Evolution of the gain with the seed power for a repetition rate of 9.2 MHz and a cooling water temperature of 5 °C.

between 47 dB and 53 dB, taking into account the uncertainty of the beam sizes. This value is close to the experimental one, and it indicates that the influence of nonradiative effects such as upconversion have a weak influence in our configuration. This is possible thanks to the low doping concentration of our sample and to the efficient cooling system.

Finally, we used the pulse picker in order to decrease the pulse repetition rate down to 200 kHz. The amplifier was then injected by an average power of 50 mW. Operating at a water temperature of 5 °C, the amplifier gave an output power up to 10 W. It corresponds to a peak power of 2.3 MW and a pulse energy of 50 μJ. The spatial profile of the output beam is shown in Fig. 5, and the output beam quality M^2 factor was 1.4.

4. CONCLUSION

In this study, different pumping wavelengths and doping concentrations of Nd:YVO$_4$ were compared theoretically. Taking into account the influence of fluorescence quenching, ETU, and the temperature dependency of the emission cross section at 1064 nm, we evaluated the potential of Nd:YVO$_4$ crystals for high gain amplifier design under 808, 880, and 888 nm. First, we have shown the significant decrease of the effective excited state lifetime with the doping concentration due to concentration quenching and ETU. This demonstrates the interest of low doping concentration, which implies the use of 808 nm despite a higher quantum defect than at 880 or 888 nm. Indeed, as nonradiative transition rates strongly increase with the doping concentration, we showed that the overall heat load is counterintuitively lower at 808 nm than at 880 or 888 nm even at significant extraction efficiency, providing that high population inversion is requested. The small signal gain coefficient evolution with the pumping rate was also studied, accounting for the upper level population depletion by nonradiative transitions and the influence of temperature on the emission cross section for the laser transition. This study shows a maximum gain coefficient found for 808 nm pumping more than 40% and 55% higher than for 880 and 888 nm pumping. For high pumping rates, the gain coefficient even starts decreasing because of the influence of temperature on the emission cross section. Finally, we have underlined the strong impact of the crystal thermal mounting and cooling system quality on performance. In order to demonstrate the advantage of 808 nm pumping and low doping concentration, we illustrated these theoretical guidelines with a high gain single stage, single pass amplifier pumped at 808 nm and using a low doping concentration of 0.1%. We obtained output powers ranging from 8.9 to 24.2 W for a seeding power between 26 mW and 3.5 W for a cooling water temperature of 5 °C. An extraction efficiency near 50% was reached at maximum seed power. A single pass small signal gain over 45 dB was measured in this system. At 200 kHz, 50 μJ pulses were produced with a peak power above 2 MW and an extraction efficiency around 25%. By tuning the cooling water temperature, we showed the large sensibility of the Nd:YVO$_4$ amplifier to the temperature, demonstrating that the cooling has to be designed carefully in order to exploit this gain medium at its full potential. Our system performance is close to what can be obtained with a regenerative amplifier but with a much simpler design in a single stage and single pass amplifier. Compared to a fiber amplifier, it has the advantage of a much higher limit in

terms of peak power, thanks to the large signal beam diameter.

REFERENCES

1. D. J. Richardson, J. Nilsson, and W. A. Clarkson, "High power fiber lasers: current status and future perspectives," J. Opt. Soc. Am. B **27**, B63–B92 (2010).
2. D. N. Papadopoulos, S. Forget, M. Delaigue, F. Druon, F. Balembois, and P. Georges, "Passively mode-locked diode-pumped Nd:YVO$_4$ oscillator operating at an ultralow repetition rate," Opt. Lett. **28**, 1838–1840 (2003).
3. U. Wegner, J. Meier, and M. J. Lederer, "Compact picosecond mode-locked and cavity-dumped Nd:YVO$_4$ laser," Opt. Express **17**, 23098–23103 (2009).
4. M. Siebold, M. Hornung, J. Hein, G. Paunescu, R. Sauerbrey, T. Bergmann, and G. Hollemann, "A high-average-power diode-pumped Nd:YVO$_4$ regenerative laser amplifier for picosecond-pulses," Appl. Phys. B **78**, 287–290 (2004).
5. M. Luehrmann, C. Theobald, R. Wallenstein, and J. A. L'huillier, "High energy cw-diode pumped Nd:YVO$_4$ regenerative amplifier with efficient second harmonic generation," Opt. Express **17**, 22761–22766 (2009).
6. J. Kleinbauer, R. Knappe, and R. Wallenstein, "13 W picoseconds Nd:GdVO$_4$ regenerative amplifier with 200 kHz repetition rate," Appl. Phys. B **81**, 163–166 (2005).
7. A. Agnesi, L. Carr, F. Pirzio, D. Scarpa, A. Tomaselli, G. Reali, C. Vacchi, and C. Braggio, "High-gain diode-pumped amplifier for generation of microjoule-level picosecond pulses," Opt. Express **14**, 9244–9249 (2006).
8. G. Turri, H. P. Jenssen, F. Cornacchia, M. Tonelli, and M. Bassi, "Temperature-dependent stimulated emission cross section in Nd^{3+}:YVO$_4$ crystals," J. Opt. Soc. Am. B **26**, 2084–2088 (2009).
9. X. Délen, F. Balembois, and P. Georges, "Temperature dependence of the emission cross section of Nd:YVO$_4$ around 1064 nm and consequences on laser operation," J. Opt. Soc. Am. B **28**, 972–976 (2011).
10. Y. Sato and T. Taira, "Temperature dependencies of stimulated emission cross section for Nd-doped solid-state laser materials," Opt. Mater. Express **2**, 1076–1087 (2012).
11. Y. F. Chen, C. C. Liao, Y. P. Lan, and S. C. Wang, "Determination of the Auger upconversion rate in fiber-coupled diode end-pumped Nd:YAG and Nd:YVO$_4$ crystals," Appl. Phys. B **70**, 487–490 (2000).
12. Z. Huang, Y. Huang, Y. Chen, and Z. Luo, "Theoretical study on the laser performances of Nd^{3+}:YAG and Nd^{3+}:YVO$_4$ under indirect and direct pumping," J. Opt. Soc. Am. B **22**, 2564–2569 (2005).
13. L. Meilhac, G. Pauliat, and G. Roosen, "Determination of the energy diffusion and the Auger upconversion constants in a Nd:YVO$_4$ standing wave laser," Opt. Commun. **203**, 341–347 (2002).
14. X. Délen, F. Balembois, O. Musset, and P. Georges, "Characteristics of laser operation at 1064 nm in Nd:YVO$_4$ under diode pumping at 808 and 914 nm," J. Opt. Soc. Am. B **28**, 52–57 (2011).
15. S. Guy, C. L. Bonner, D. P. Shepherd, D. C. Hanna, and A. C. Tropper, "High-inversion densities in Nd:YAG: upconversion and bleaching," IEEE J. Quantum Electron. **34**, 900–909 (1998).
16. C. Jacinto, S. L. Oliveira, T. Catunda, A. A. Andrade, J. D. Myers, and M. J. Myers, "Upconversion effect on fluorescence quantum efficiency and heat generation in Nd^{3+}-doped materials," Opt. Express **13**, 2040–2046 (2005).
17. R. Lavi, S. Jackel, Y. Tzuk, M. Winik, E. Lebiush, M. Katz, and I. Paiss, "Efficient pumping scheme for neodymium-doped materials by direct excitation of the upper lasing level," Appl. Opt. **38**, 7382–7385 (1999).
18. L. McDonagh, R. Wallenstein, R. Knappe, and A. Nebel, "High-efficiency 60 W TEM$_{00}$ Nd:YVO$_4$ oscillator pumped at 888 nm," Opt. Lett. **31**, 3297–3299 (2006).

19. D. Sangla, M. Castaing, F. Balembois, and P. Georges, "Highly efficient Nd:YVO$_4$ laser by direct in-band diode pumping at 914 nm," Opt. Lett. **34**, 2159–2161 (2009).

20. Y. F. Chen, T. M. Huang, C. F. Kao, C. L. Wang, and S. C. Wang, "Optimization in scaling fiber-coupled laser-diode end-pumped lasers to higher power: Influence of thermal effect," IEEE J. Quantum Electron. **33**, 1424–1429 (1997).

21. J. Morikawa, C. Leong, T. Hashimoto, T. Ogawa, Y. Urata, S. Wada, M. Higuchi, and J. Takahashi, "Thermal conductivity/ diffusivity of Nd^{3+} doped GdVO$_4$, YVO$_4$, LuVO$_4$, and Y$_3$Al$_5$O$_{12}$ by temperature wave analysis," J. Appl. Phys. **103**, 063522 (2008).

22. Y. Sato and T. Taira, "The studies of thermal conductivity in GdVO$_4$, YVO$_4$, Y$_3$Al$_5$O$_{12}$ measured by quasi-one dimensional flash method," Opt. Express **14**, 10528–10536 (2006).

23. S. Chénais, S. Forget, F. Druon, F. Balembois, and P. Georges, "Direct and absolute temperature mapping and heat transfer measurements in diode-end-pumped Yb:YAG," Appl. Phys. B **79**, 221–224 (2004).